Electronic supplementary information

"Pulverization-Reaggregation"-Induced *In-Situ* Pore Expanding in Carbon for Fast Potassium Storage

Chao Geng, Yaxin Chen, Zongfu Sun, Weijia Guo, Jiangmin Jiang, Yongli Cui, Yueli Shi, Quanchao Zhuang and Zhicheng Ju**

School of Materials Science and Physics, China University of Mining and Technology, Xuzhou 221116, P. R. China.

*Correspondence authors. Email: chenyxcumt@163.com (Yaxin Chen), or juzc@cumt.edu.cn (Zhicheng Ju)

Experimental section

Fabrication of CNS products: Typically, pitch and basic flake magnesium carbonate ($4MgCO_3 \cdot Mg(OH)_2 \cdot 4H_2O$) were dissolved in ethylene glycol solution at a mass ratio of 1:5, and the mixture was ball-milled for 4h. The mixture was heated at 350 °C for 2 h, followed by carbonization at the target temperature for 2 h in Ar with a heating rate of 5 °C min^{-1}. After carbonization, the black carbon/MgO composite was washed using 1M HCl for 8h at room temperature to remove the MgO, and then washed with distilled water until it appeared neutral. Finally, the produce was dried in a vacuum oven at 80 °C for 8 h to obtain porous carbon nanosheets, denoted as CNS-T, where T refers to the carbonization temperature. In addition, the same treatment was subjected for pitch/basic zinc carbonate, pitch/basic nickel carbonate and pitch/basic cupric carbonate.

Materials Characterizations: The morphology of the products was characterized by field emission scanning electron microscopy (Field-emission SEM, TESCAN MAIA3), and high-resolution transmission electron microscopy (HRTEM, TECNAI G2 F20). The thickness of products was tested by Atomic Force Microscopy (AFM, Dimension Icon) in tapping mode. Pore structure analysis was conducted via N_2 adsorption/desorption isotherms collected on a micromeritics ASAP 2020. Electronic conductivity was tested using FM100GH powder resistivity tester under a test pressure of 2 MPa. The structural information of the products was collected using X-ray diffraction (XRD, Rigaku D/max-2500B2$^+$/PCX system, Cu Kα radiation) and Raman spectroscopy (Aramis system, Jobin Yvon). XPS spectroscopy data was recorded on AXIS-ULTRA DLD-600W. Electron paramagnetic resonance (EPR) spectroscopy was obtained from Bruker EMX plus.

Electrochemical measurements: The electrochemical properties of the products were tested using CR2025 coin cells. The working electrode was prepared by blending the mixture of active materials, acetylene black, and carboxymethylcellulose (CMC) with a mass ratio of 8:1:1 in deionized water. Potassium foil was used as the counter electrode. The electrolyte was 0.8 mol L^{-1} KPF_6 dissolved in ethylene carbonate (EC)

and diethyl carbonate (DEC) (1:1 volume ratio). Glass fiber membrane (Whatman GF/C 47 mm) was used as the separator. Charge-discharge and galvanostatic intermittent titration technique (GITT) measurements were measured using the CT2001A land battery test system over a voltage window of 0.01-3.00 V. Cyclic voltammetry (CV) curves and electrochemical impedance spectroscopy (EIS, frequency range 100 kHz ~ 10 MHz, amplitude 5 mV) were obtained on a CHI760D electrochemical workstation (Shanghai Chenhua).

DFT calculation: In this work, periodic density functional theory (DFT) calculations were conducted using the Vienna Ab-initio Simulation Package (VASP, version 5.4.4).[1] Core electron states were represented by the projector-augmented wave (PAW) method with the generalized gradient approximation Perdew–Burke–Ernzerhof (PBE) functional under the Generalized Gradient Approximation (GGA).[2] The plane waves energy cutoff was chosen to be 600 eV, to ensure the total energy was converged to 0.001 eV per atom. The Brillouin zone was sampled with a mesh by Monkhorst packing. Convergence tolerances of energy and ionic convergence criterion were set to 10-6 eV and 0.01 eV/Å. In the calculation, the standard spin is used as the initial spin, and DFT-D3 is used to process van der Waals forces.

Supplementary figures:

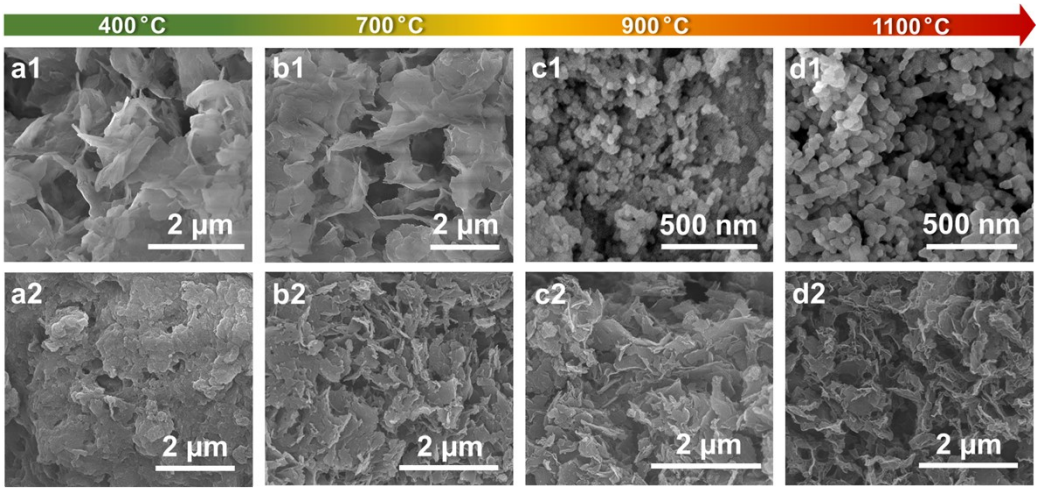

Fig. S1 SEM images of basic magnesium carbonate at (a1) 400, (b1) 700, (c1) 900 and (d1) 1100 °C, respectively. SEM images of (a2) CNS-400, (b2) CNS-700, (c2) CNS-900 and (d2) CNS-1100.

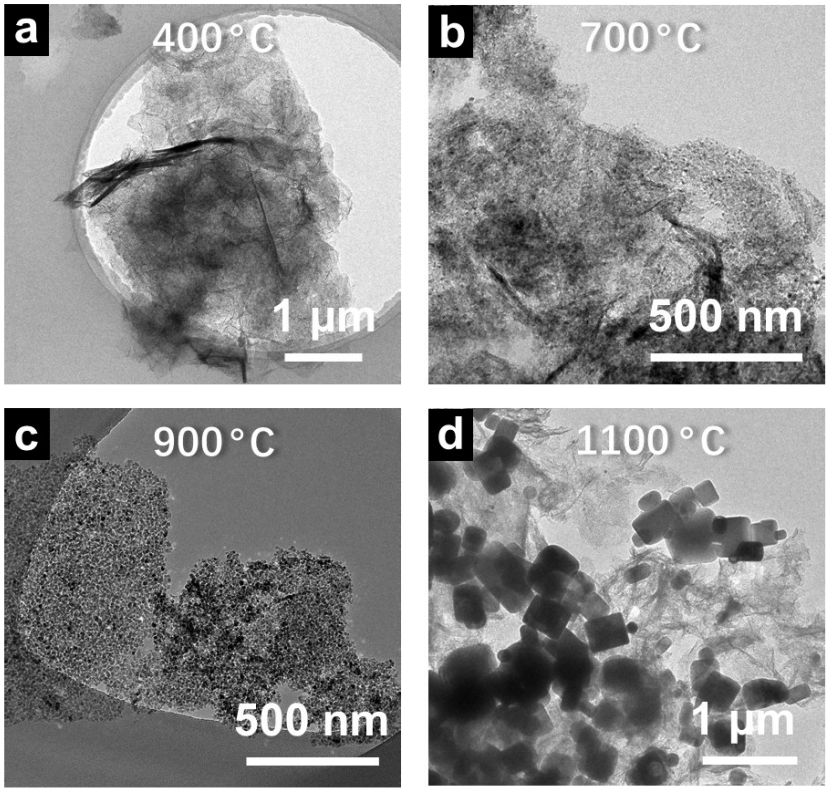

Fig. S2 TEM images of (b1) CNS-400, (c1) CNS-700, (d1) CNS-900 and (e1) CNS-1100 before the removal of template.

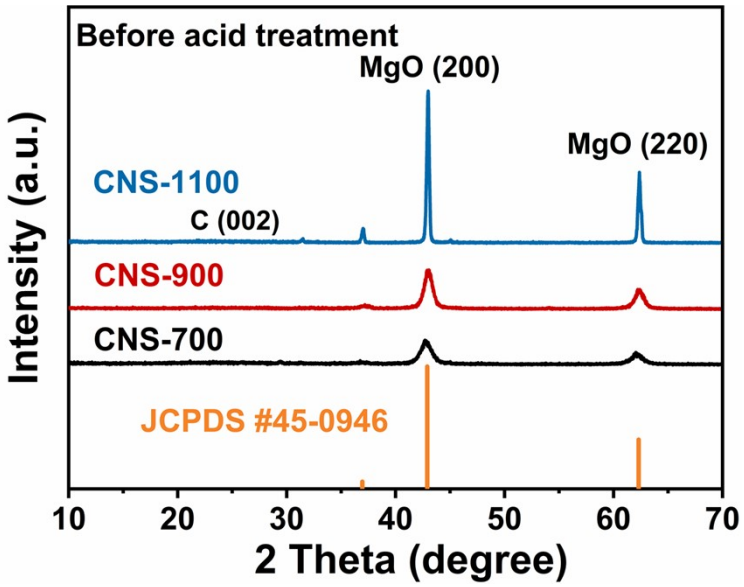

Fig. S3 XRD patterns of CNS before the removal of template

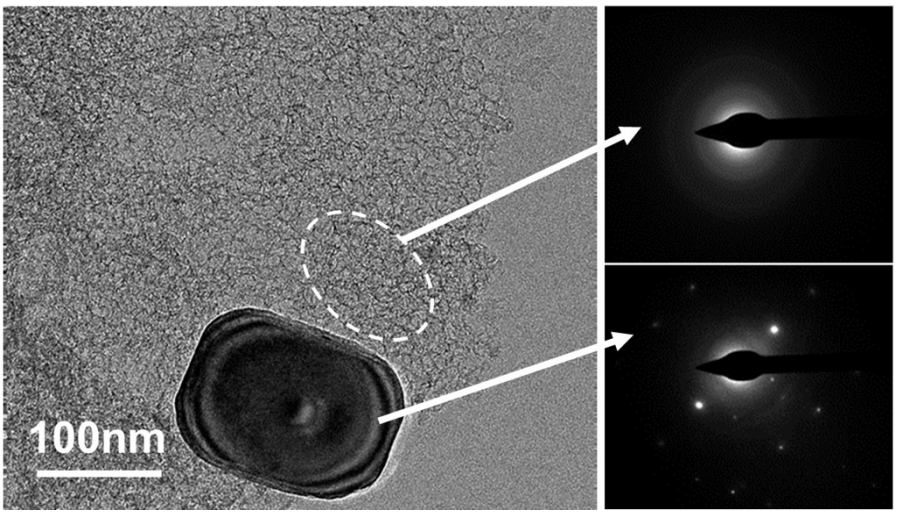

Fig. S4 TEM images and selected area electron diffraction of CNS-1100 before the removal of template.

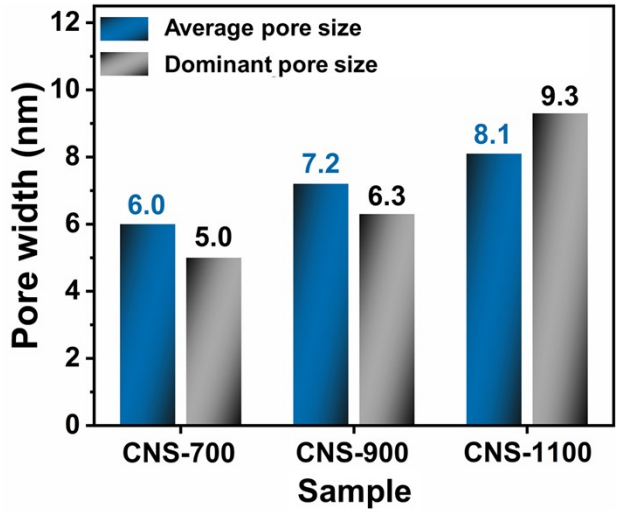

Fig. S5 Average and dominant pore size distribution of CNS.

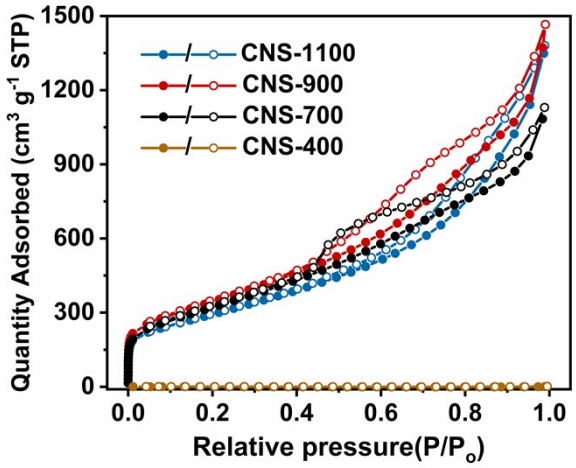

Fig. S6 N2 adsorption-desorption isotherms curves of CNS

Table S1 BET specific surface area and pore structure parameters of CNS

Sample	S_{BET} (m^2 g^{-1})	V_t (cm^3 g^{-1})	V_{mic} (cm^3 g^{-1})
CNS-400	1.1	0.0026	0.0018
CNS-700	1175.8	1.7480	0.0734
CNS-900	1264.5	2.1215	0.0592
CNS-1100	1065.6	2.1355	0.0002

S_{BET}: BET surface area. V_{mic}: t-Plot micropore volume. V_t: total pore volume.

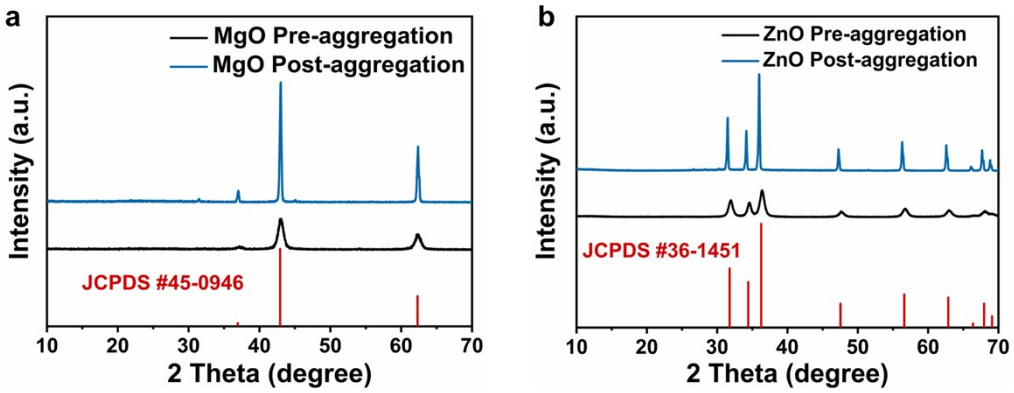

Fig. S7 The variation of (a) pitch/basic magnesium carbonate and (b) pitch/basic zinc carbonate which are detected by XRD patterns.

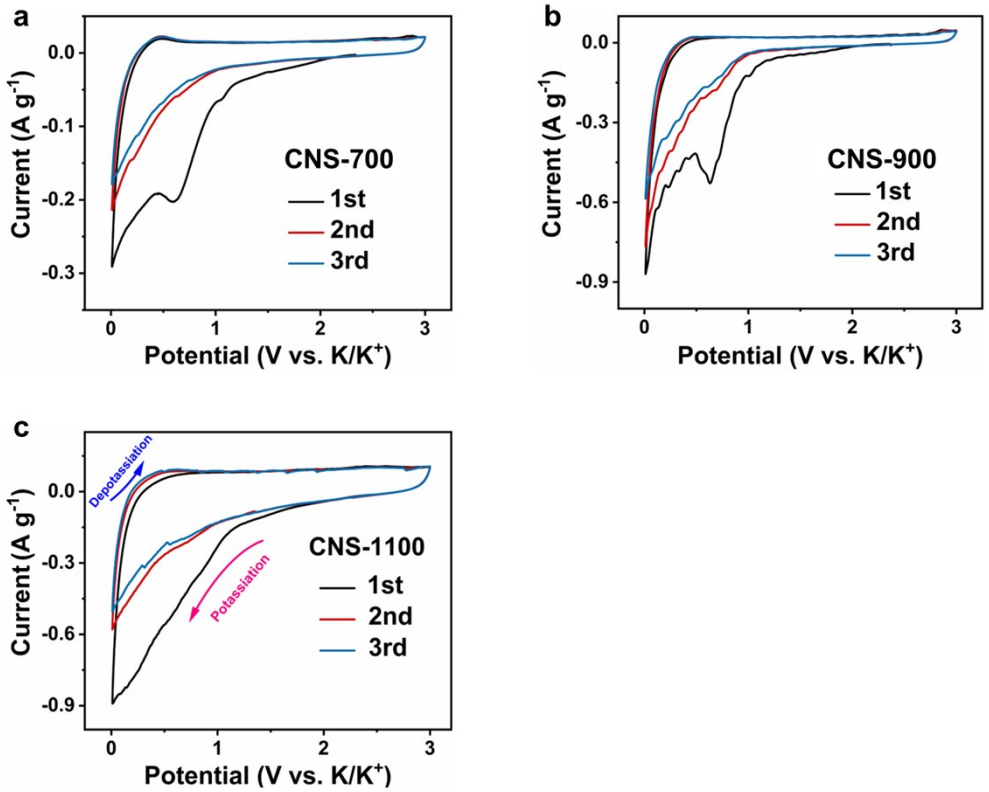

Fig. S8 CV curves of initial 3 cycles at 0.1 mV s^{-1} of (a) CNS-700, (b) CNS-900 and (c) CNS-1100 electrodes.

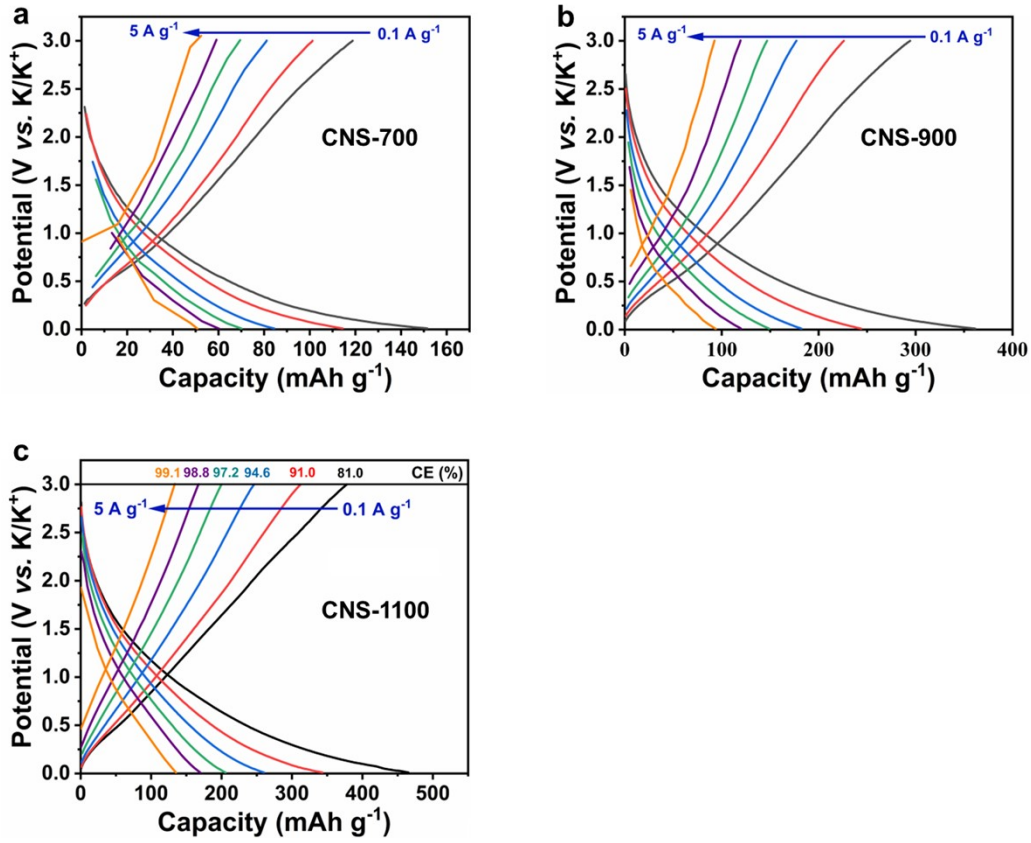

Fig. S9 Galvanostatic charge/discharge profiles from 0.1 to 5 A g^{-1} of (a) CNS-700, (b) CNS-900 and (c) CNS-1100 electrodes.

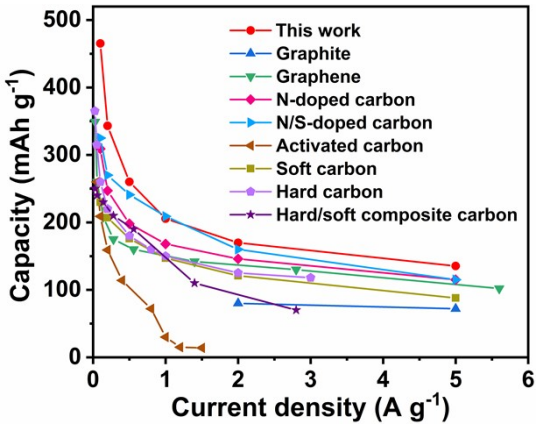

Fig. S10 Comparison of different defective carbon anode materials of PIBs

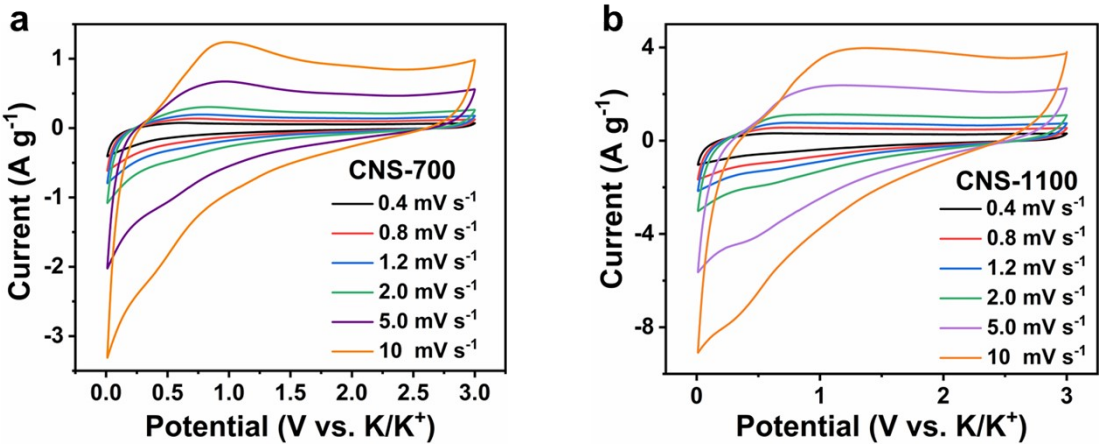

Fig. S11 CV curves from 0.4 to 10 mV s^{-1} for (a) CNS-700 and (b) CNS-1100, respectively.

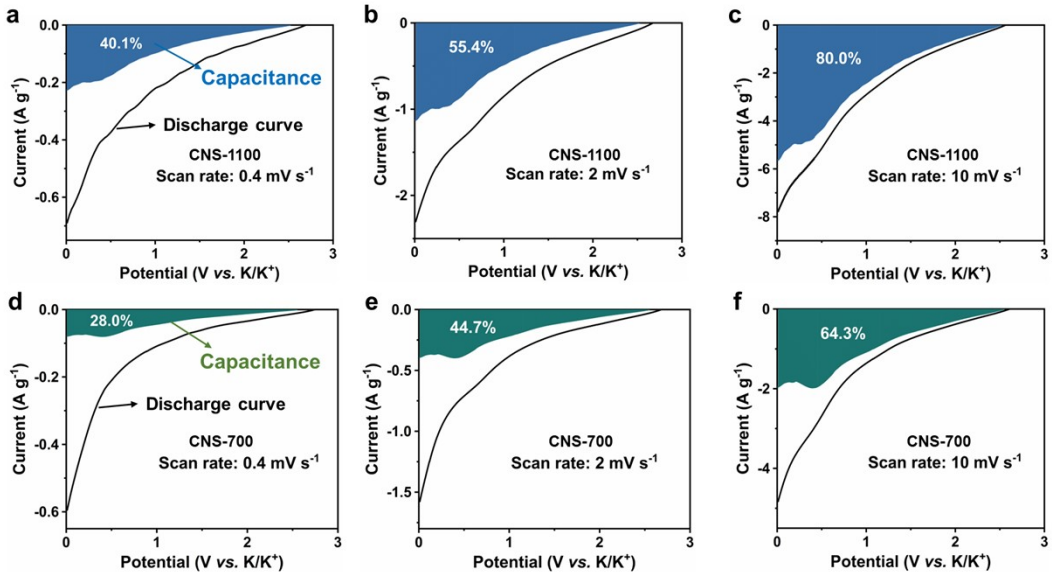

Fig. S12 Separating the surface-dominated capacity contribution in the cathodic scan at 0.4, 2 and 10 mV s^{-1} for (a-c) CNS-1100 and (d-f) CNS-700, respectively.

Note: We quantitatively calculated the "capacitive capacity" and by analyzing the change of the current (i) along with the sweep rate (v) of cyclic voltammetry (CV) responds at scan rates from 0.4 to 10 mV s^{-1}. To quantify the surface capacitance contribution and the contribution of diffusion control in the overall capacity, the current (i) versus the scan rate (v) was:[3-5]

$$i = av^{b}$$

where a and b are adjustable parameters, and i and v denote the peak current and scan rate, respectively.

The contributions of diffusion control and surface capacitance can be expressed by the following equation:

$$i = k_1 v + k_2 v^{1/2}$$

In this equation, $k_1 v$ represent the capacitive contribution, and $k_2 v^{1/2}$ represents the diffusion-controlled contribution.

And this equation can be rearranged to the equation as follows for easy analysis.

$$i/v^{1/2} = k_1 v^{1/2} + k_2$$

k_1 and k_2 can be determined by fitting a straight line of $i/v^{1/2}$ vs. $v^{1/2}$, in which k_1 is the slope and k_2 is the y-intercept.

Specific processing method: Using *excel* software, the current *i* at different scan rates is divided by the corresponding $v^{1/2}$, which yields a column of data $i/(v^{1/2})$. Then A nonlinear fit is performed for different root scan rates. Therefore, k_1 can be derived by using the SLOPE function, and k_2 can be determined by using the INTERCEPT function. As shown in Table R2, take the CNS-1100 as an example, k_1 and k_2 values were calculated in the range of 0.01-3V. After obtaining the k_1v and $k_2v^{1/2}$ curves, the area enclosed by them is divided by the area of the original CV curve, respectively, to obtain the capacitance contribution rate and the diffusion contribution rate.

Table S2 k_1 and k_2 values in the range of 0.01-3V for CNS-1100.

Potential (V, discharge)	**k_1 (10^{*-5})**	**k_2 (10^{*-5})**
3.0	**0.399**	**0.312**
2.5	**-0.004**	**-0.066**
2.0	**-0.104**	**-0.144**
1.5	**-0.233**	**-0.225**
1.0	**-0.434**	**-0.376**
0.5	**-0.781**	**-0.573**
0.01	**-1.014**	**-1.352**

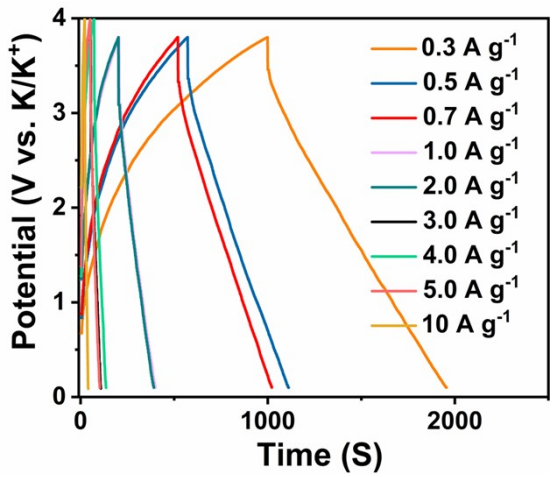

Fig. S13 Charge and discharge curves of CNS//AC at different current densities.

Reference

1. P. P. John, B. Kieron, E. Matthias, Rev. Lett. 1996, **77**, 3865.
2. G. Kresse, D. Joubert, Phys. Rev. B, 1999, **59**, 1758-1775.
3. J. Wang, J. Polleux, J. Lim and B. Dunn, J. Phys. Chem. C, 2007,**111**, 14925-14931.
4. J. Cao, L. Wang, D. Li, Z. Yuan, H. Xu, J. Li, R. Chen, V. Shulga, G. Shen and W. Han, *Adv Mater*, 2021, **33**, 2101535.
5. Y. An, Y. Tian, Q. Man, H. Shen, C. Liu, Y. Qian, S. Xiong, J. Feng and Y. Qian, *ACS Nano*, 2022, **16**, 6755-6770.